Electronic Supplementary Material (ESI) for Journal of Materials Chemistry A.

Full Volmer-Heyrovsky reaction catalyst based on sulfur vacancy structure optimization

Bin Tian,[a] Ligang Sun[b]* Zhiyuan Zeng[a]* and Derek Ho[a,c]*

[a]Department of Materials Science and Engineering, City University of Hong Kong, Kowloon, Hong Kong, China

[b]School of Science, Harbin Institute of Technology, Shenzhen, China

[c]Hong Kong Center for Cerebro-Cardiovascular Health Engineering, Hong Kong, China

Experimental section

Chemical reagents

All chemical reagents were used directly without further purification. Ferrous chloride ($FeCl_2 \cdot 4H_2O$, 99.8%, Acros), iron nitrate, nonahydrate ($Fe(NO_3)_3 \cdot 9H_2O$, 99%, Acros), thiourea (CH_4N_2S, 99.8%), phosphorus pentasulfide (P_2S_5, 99%, Aladdin) ethanediamine (EDA, 99%, Aladdin), ethylene glycol (EG, 99%, Aladdin), potassium hydroxide (KOH, 99%, Aladdin), sulfuric acid (H_2SO_4, 98%, Aladdin), ethyl alcohol (C_2H_6O, 95%), cetyl trimethyl ammonium bromide (CTAB, 98%, Aladdin) and 20% Pt/C catalyst (Shanghai Macklin Biochemical Co., Ltd).

Preparation of pristine FeS (p-FeS)

As a comparison, a baseline FeS (p-FeS) sample was prepared, based on a previously reported method.[S1] 1.97 mmol of ferrous chloride powder and 2.63 mmol of thiourea were dissolved in ethylene glycol under vigorous stirring to form a homogeneous solution at 318 K. Then, 2 mL of sodium citrate aqueous solution (0.1 wt%) was dropped gradually, then transferred to a Teflon-lined stainless-steel autoclave and heated at 493 K for 15 h. After naturally cooling down to room temperature, the FeS nanosheets was obtained by consecutively washing several times with ethanol and deionized water, then dried for 8 h in a vacuum oven at 323 K.

Material characterizations

The crystal structures of the as-prepared samples were characterized by XRD (Bruker, D2 Phaser) using Cu kα radiation with a wavelength of 1.54 Å. Raman

spectrum was collected using a spectrophotometer (WITec, alpha 300 access) with a 532 nm laser. The morphology of samples was characterized by TEM (JEOL 2100F) and SEM (JEOL JSM-6335F). XPS (Thermo Escalab 250Xi) was used to analysis the elemental valence and surface electronic structure of the chemical products, with binding energies referenced to adventitious carbon at 284.8 eV. Thermogravimetric analysis (TGA, SDT Q600) of the nanofibers was conducted in air at a heating rate of 10 ℃ min^{-1}. The BET surface areas of the catalysts were measured by single-point N_2 adsorption/desorption cycles using an ASAP 2020 porosity and specific surface area analyzer. EPR spectra were collected at room temperature using a Bruker RPE Elexsys E500 spectrometer equipped with a SHQ with X band frequency in a continuous wave cavity. Spectra were recorded with a modulation amplitude of 3510 G, a modulation frequency of 100 kHz and a microwave power of about 20 mW. Inductively coupled plasma optical emission spectrometer (ICP-OES) was performed on Agilent 5110. In-situ attenuated total reflectance surface-enhanced infrared absorption spectroscopy (ATR-SEIRAS) experiments were collected with 4 cm^{-1} resolution and at least 128 coadded scans using a FTIR spectrometer (Nicolet iS50, Thermo Scientific) equipped with a liquid nitrogen-cooled MCT detector.

Mass activity calculation

The mass activity of catalysts was calculated based on the polarization curves shown in Fig. 3a. In detail, the current density of OSV-FeS catalyst is 92.0 mA cm^{-2} at 200 mV, the current density of p-FeS is about 14.6 mA cm^{-2}. The mass of catalysts is 0.3 mg cm^{-2}. The calculated mass activity of OSV-FeS and p-FeS is 306 mA $mg_{catalyst}^{-}$

[1]and 48.6 A $mg_{catalyst}^{-1}$. Therefore, the mass activity of OSV-FeS is about 6.3 times compared to p-FeS.

ECSA calculation

As the double layer capacitance (C_{dl}) is proportional to the electrochemical surface area (ECSA) and determines from the corresponding cyclic voltammetry (CV) curves. The CV curves was tested with the scan rates of 25, 50, 75, 100, 150 and 200 mV s^{-1}. Then, the current density obtained from the CV curves at each scan rate was calculated by the formula $\Delta j=j_1-j_2$. $\Delta j/2$ at each scan rate was then linearly fitted by the least-squares method, and the slope value of the curve obtained was C_{dl}. Furthermore, ECSA was obtained by the equation as follow:[S2]

$$ECSA = C_{dl}/C_s.$$

where C_s is the capacitance of catalysts, which has a specific value in the range of 20-60 F cm^{-2}, and we took C_s = 40 F cm^{-2}."

Turnover frequency calculation

The turnover frequency (TOF) could be defined as the number of times of reactions per unit time for a given active site. The TOF values were calculated references previous report based on the following equation:[S3]

$$HER\ TOF = (JS)/(2nF)$$

where J is the current density (mA cm^{-2}) at specified overpotentials, S is the BET surface area [m^2 g^{-1}] of the catalyst (shown in Table S3), F is the Faraday constant (96485.3 C mol^{-1}), and n is the weight of the active materials."

DFT calculations

DFT method is employed to investigate the atomistic mechanism about the HER performance of our catalyst by using the Cambridge Sequential Total Energy Package (CASTEP) module in Materials Studio software.[S4] Generalized gradient approximation method with the Perdew-Burke-Ernzerh function (GGA-PBE) is adopted to describe the exchange and corrections of atomic interaction.[S5] The interactions between valence electrons and ionic cores is described by ultrasoft pseudo-potential method.[S6] A plane-wave basis set with a cutoff energy of 400 eV is assigned. The Brillouin zone is sampled by a Monkhorst-Pack grid.[S7] The tolerances of energy, force and displacement for structure optimization are 10^{-5} eV atom^{-1}, 0.03 eV Å^{-1} and 0.001 Å respectively. The self-consistence field (SCF) is set as 1×10^{-5} eV atom^{-1}.

The water adsorption energies (ΔE_{H_2O}) at the surface of catalysts are calculated by the following equation:

$$\Delta E_{H_2O} = E_{surf+H_2O} - E_{surf} - E_{H_2O}$$

where the E_{surf} and the E_{surf+H_2O} are the total energies of the surface before and after water adsorption. E_{H_2O} represents the energy of a free water molecule.

The Gibbs free energies for hydrogen adsorption (ΔG_{H^*}) are calculated by the following equation:

$$\Delta G_{H^*} = \Delta E_{H^*} + \Delta ZPE - T\Delta S$$

where the ΔE_{H^*}, ΔZPE, T and ΔS are the binding energy, zero-point energy (ZPE)

change, temperature, and entropy change of H* adsorption system, respectively.

The vibrational entropy of H* in the adsorbed state is generally negligible. Therefore, ΔS can be calculated by the following equation:

$$\Delta S = S_{H^*} - \frac{1}{2}S_{H_2} \approx -\frac{1}{2}S_{H_2}$$

where S_{H_2} is the entropy of gas phase H_2 at the standard conditions.

Moreover, ΔZPE can be calculated by the equation of $\Delta ZPE = ZPE_{H^*} - \frac{1}{2}ZPE_{H_2}$. Hence, the Gibbs free energy of the adsorbed state of H* can be calculated by the simplified equation:[S8]

$$\Delta G_{H^*} = \Delta E_{H^*} + 0.24\ eV$$

Two kinds of representative FeS atomistic models with (1) S vacancies (named as SV-FeS) and (2) S vacancies be occupied by O element (named as OSV-FeS) which are as obtained in our experiment, are constructed to investigate their HER performance. Structure optimizations were performed to optimize the crystal structure, with *k* points set as (4×4×2). Then the surface models with a vacuum layer of ~15 Å were built and further geometrically optimized and utilized to study their HER capacity, with *k* points set as (4×4×1).

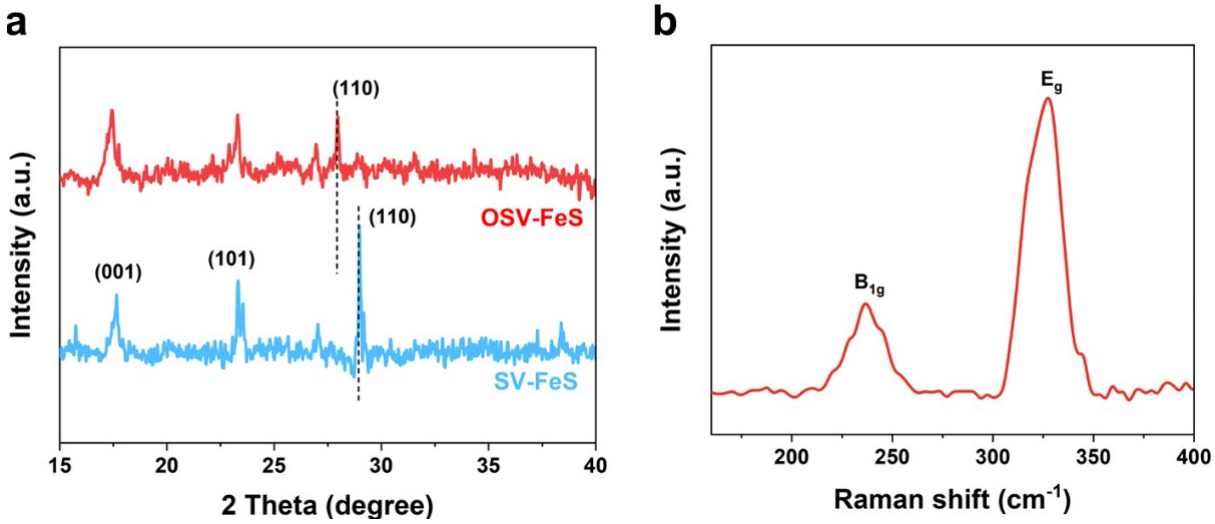

Fig. S1. (a) XRD patterns of SV-FeS and OSV-FeS and (b) Raman spectrum of the SV-FeS catalysts.

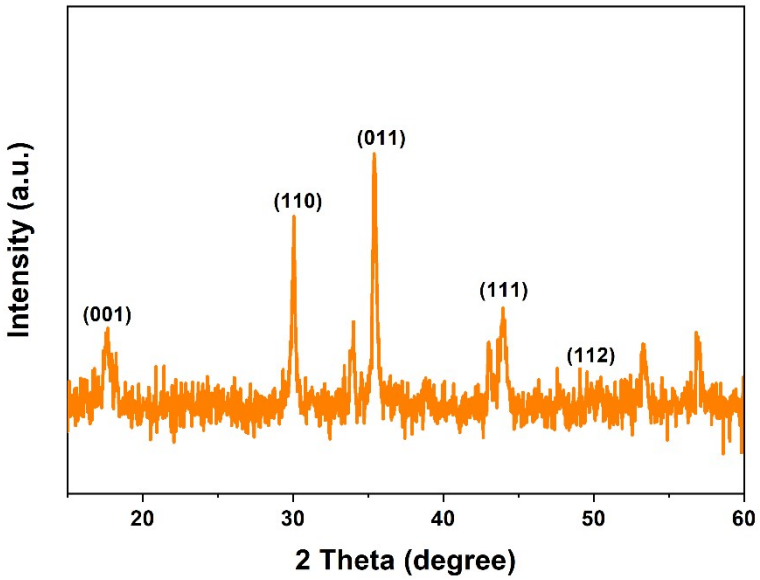

Fig. S2. XRD pattern of the p-FeS catalyst.

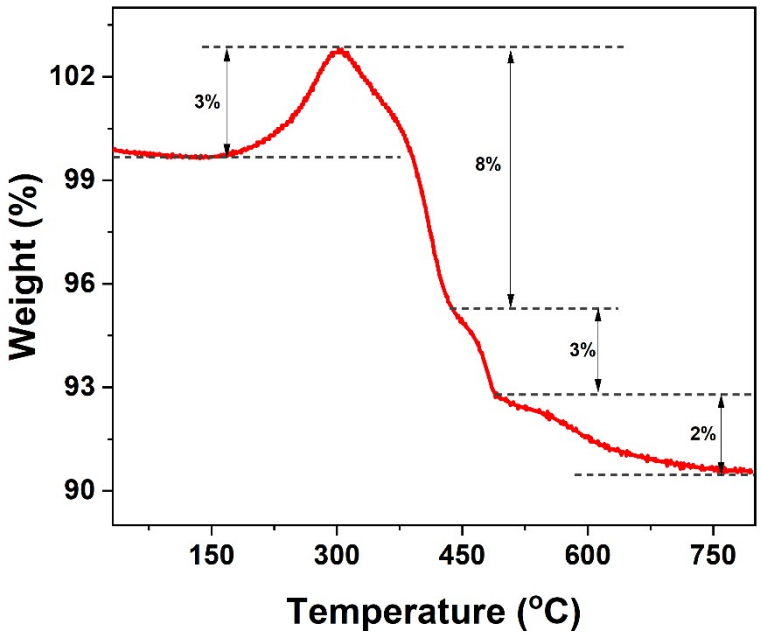

Fig. S3. Thermogravimetric curve of OSV-FeS samples.

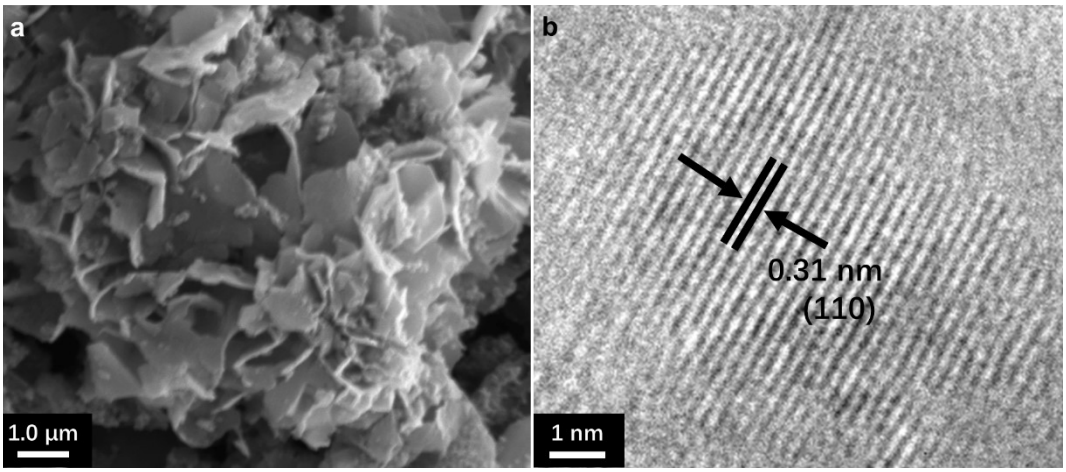

Fig. S4. (a) SEM and HRTEM images of p-FeS catalyst.

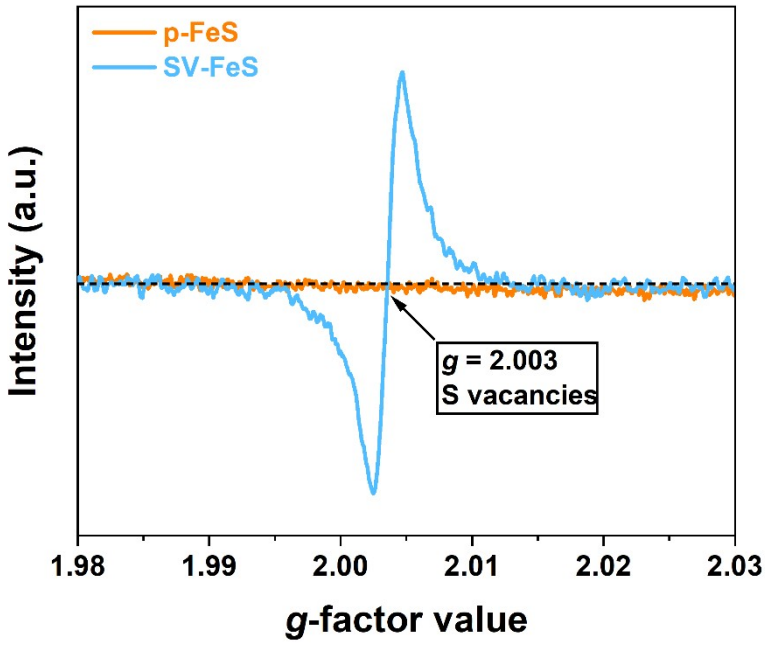

Fig. S5. EPR spectra Comparison of the p-FeS and SV-FeS catalysts.

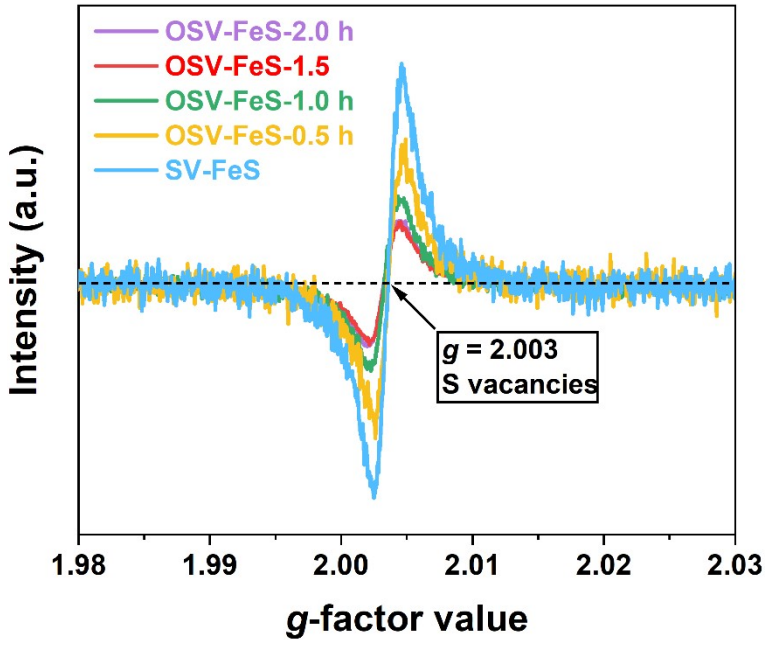

Fig. S6. EPR spectra of OSV-FeS catalysts with different electrochemical treatment time.

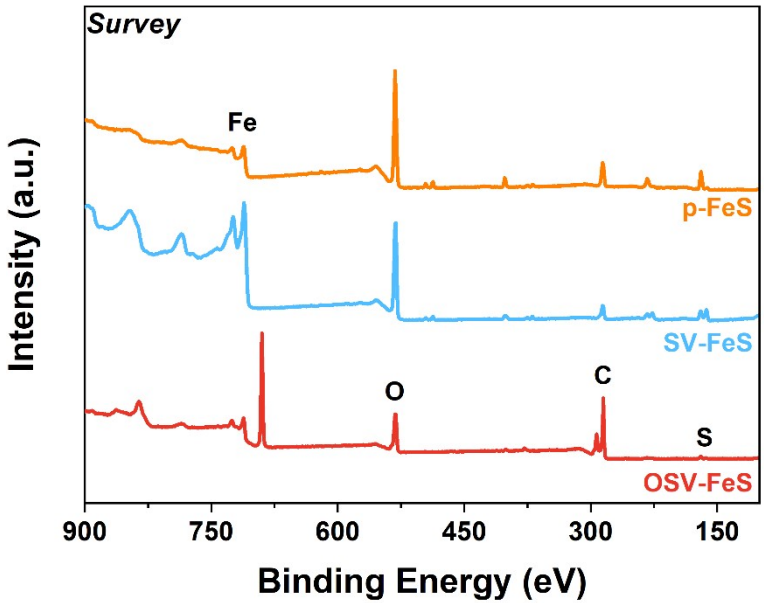

Fig. S7. XPS survey of p-FeS, SV-FeS and OSV-FeS catalysts.

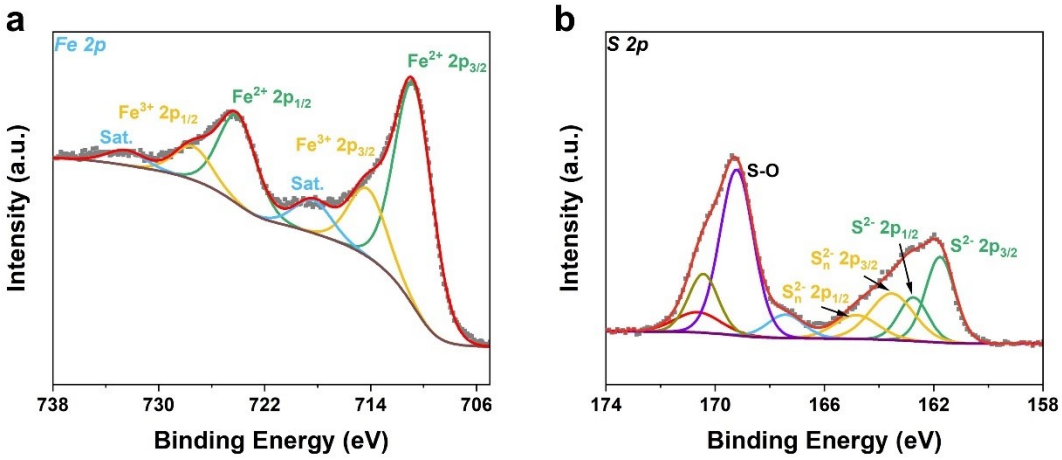

Fig. S8. XPS fine spectra of p-FeS: (a) Fe *2p* and (b) S *2p*.

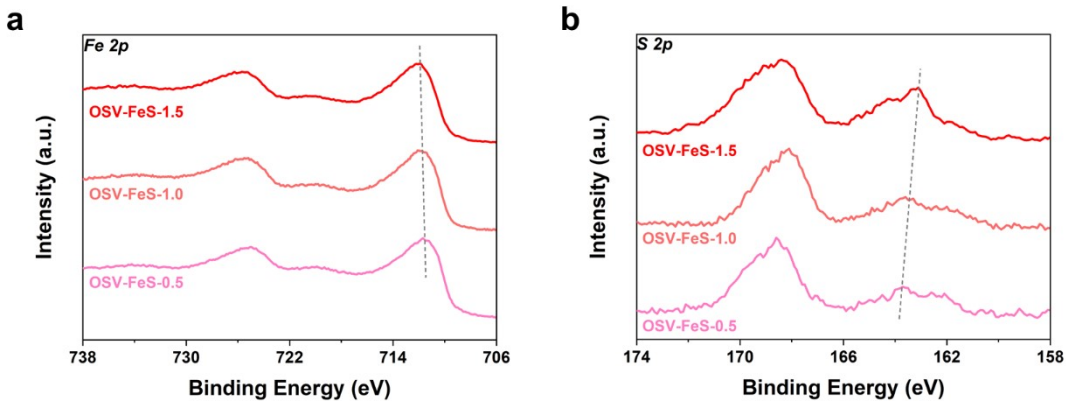

Fig. S9. XPS fine spectra of OSV-FeS catalyst with electrochemical treatment time from 0.5 to 1.5 h: (a) Fe *2p* and (b) S *2p*.

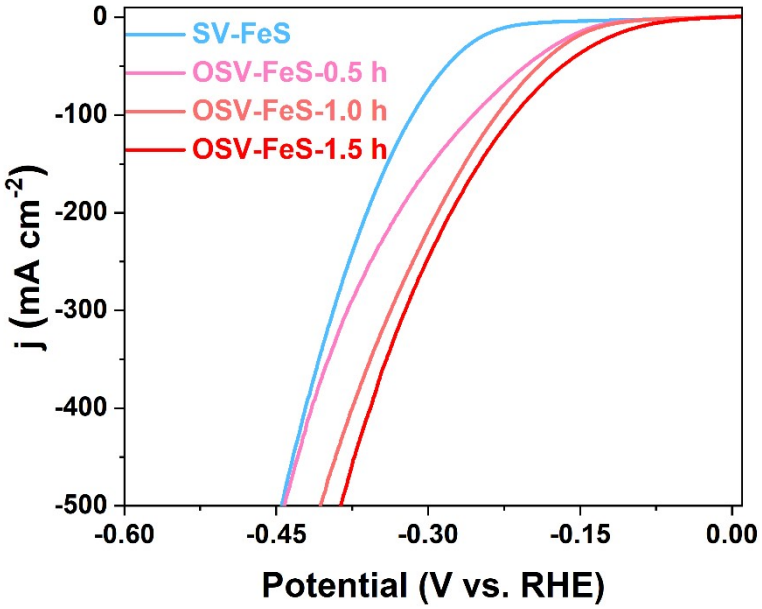

Fig. S10. Polarization curves of OSV-FeS with different electrochemical treatment time from 0 to 1.5 h.

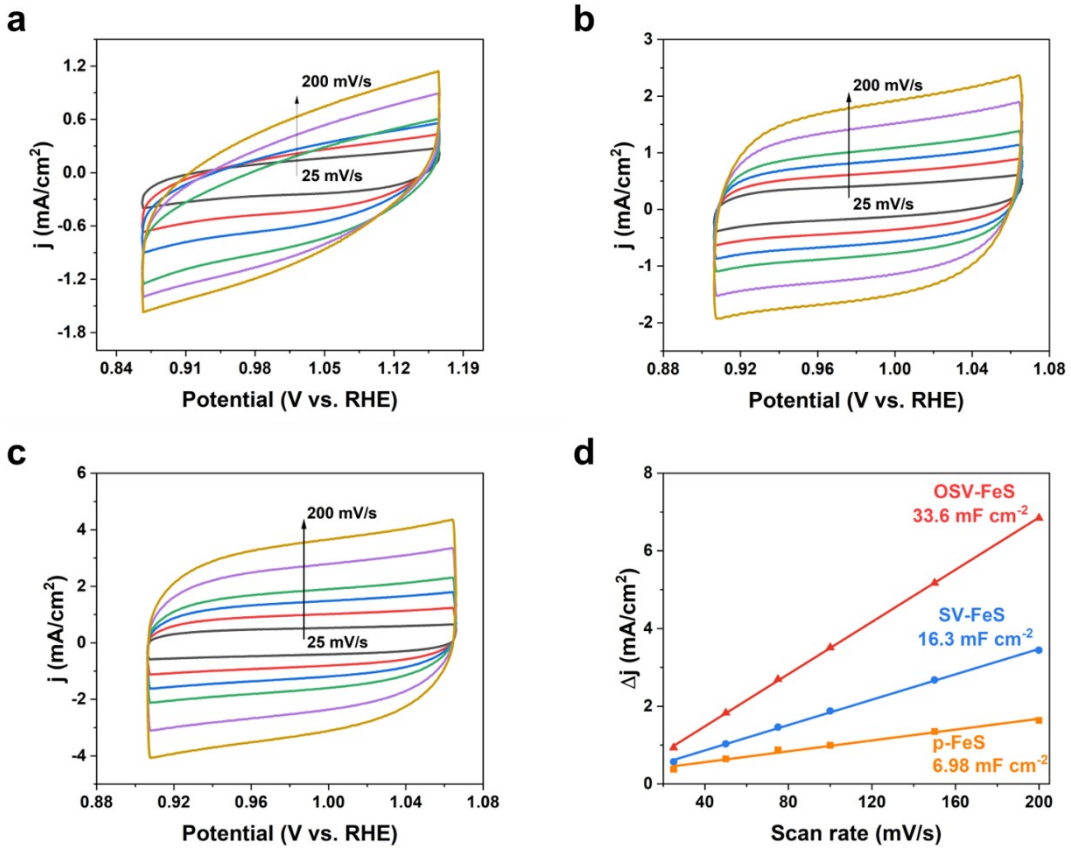

Fig. S11. Cyclic voltammograms of (a) p-FeS, (b) SV-FeS, (c) OSV-FeS in the double layer region (without Faradic process) at the scan rates of 25, 50, 75, 100, 150, 200 mV s^{-1} varying along the arrow direction. (d) C_{dl} Comparison of p-FeS, SV-FeS and OSV-FeS.

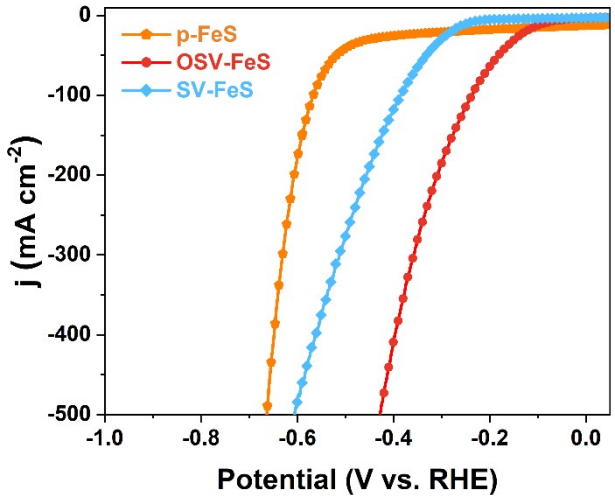

Fig. S12. ECSA normalized LSV curves of p-FeS, SV-FeS and OSV-FeS electrocatalysts.

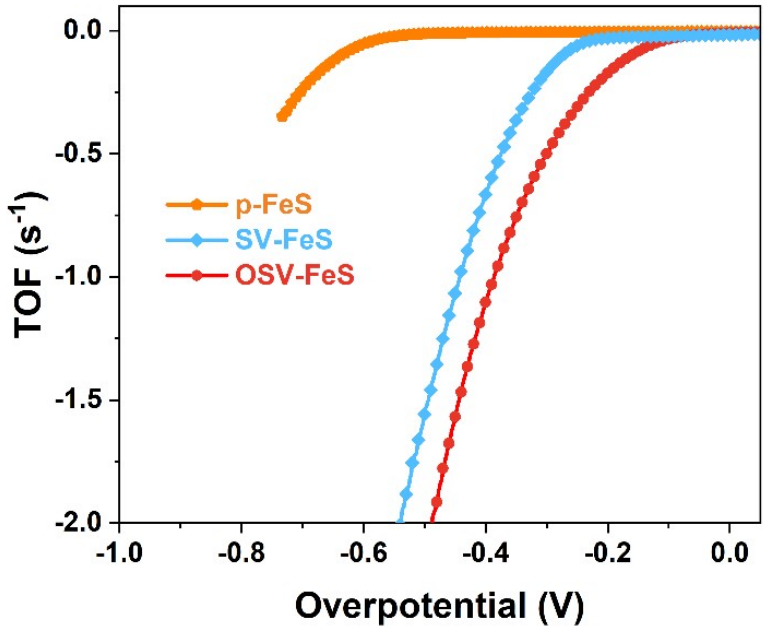

Fig. S13. TOF values of p-FeS, SV-FeS and OSV-FeS electrocatalysts.

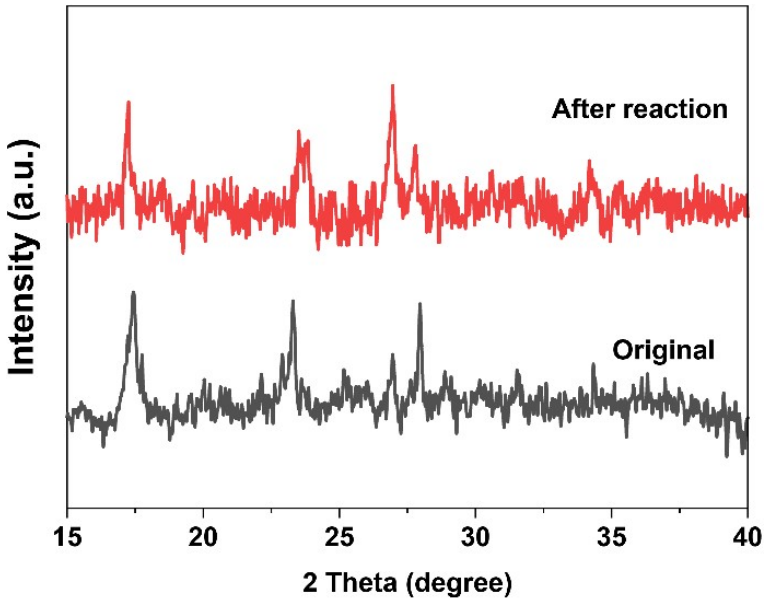

Fig. S14. XRD patterns of OSV-FeS before and after HER tests.

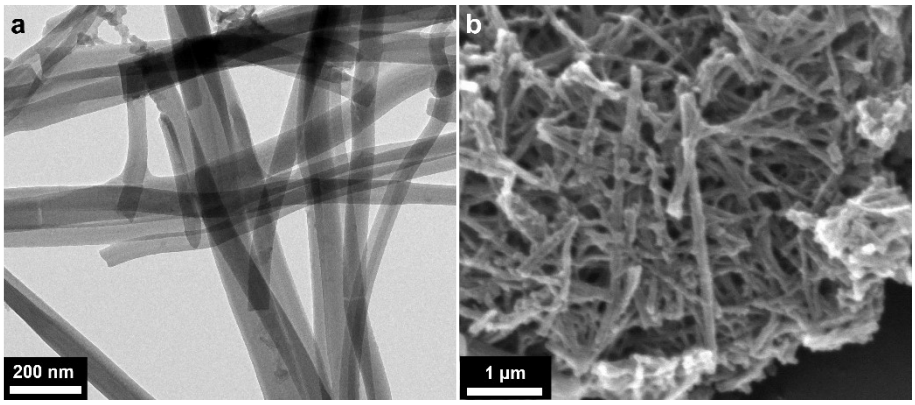

Fig. S15. (a) SEM and (b) TEM image of OVS-FeS after HER test.

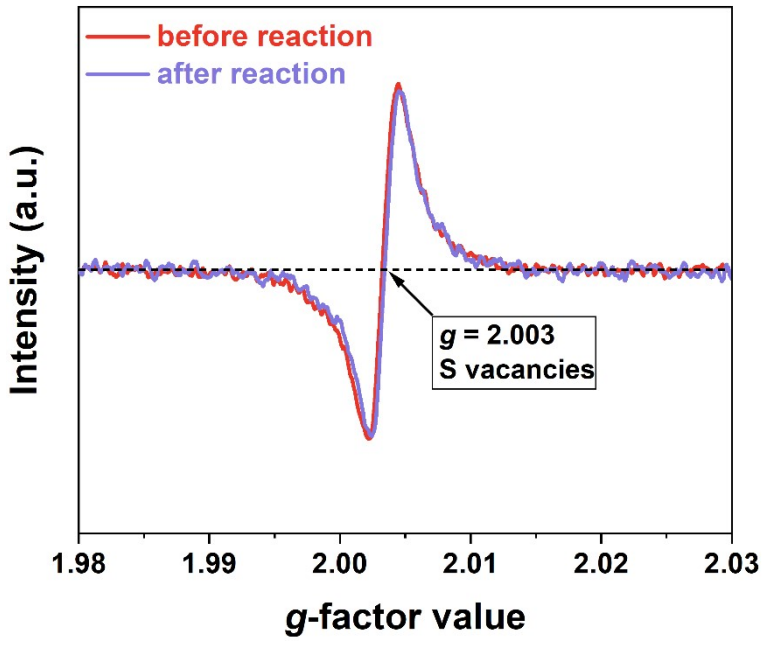

Fig. S16. EPR spectra of OSV-FeS catalyst and after stability test.

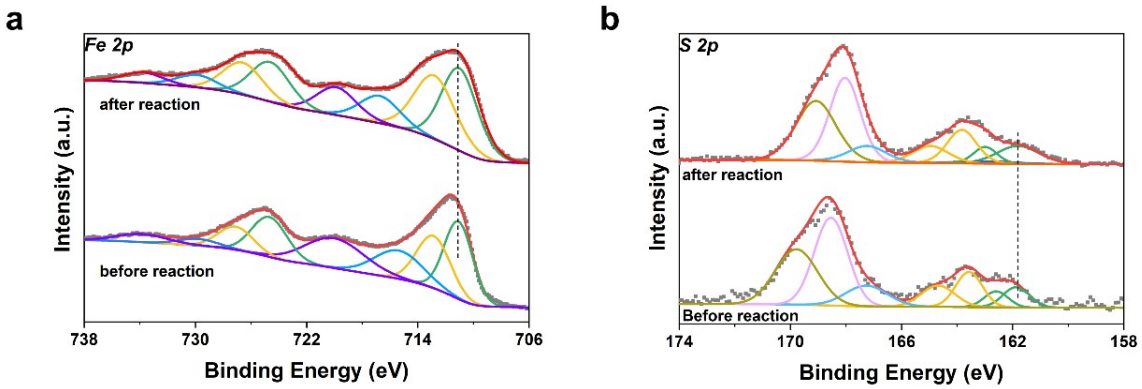

Fig. S17. (a) Fe *2p* and (b) S *2p* XPS fine spectra of the OSV-FeS catalyst before and after stability test.

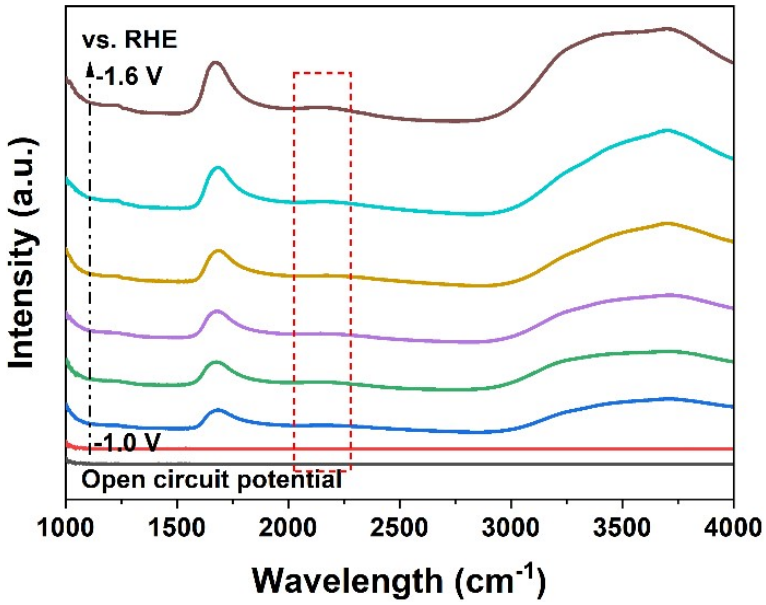

Fig. S18. In-situ ATR-SEIRAS spectra of OSV-FeS in N_2-saturated 1 M KOH for HER at room temperature.

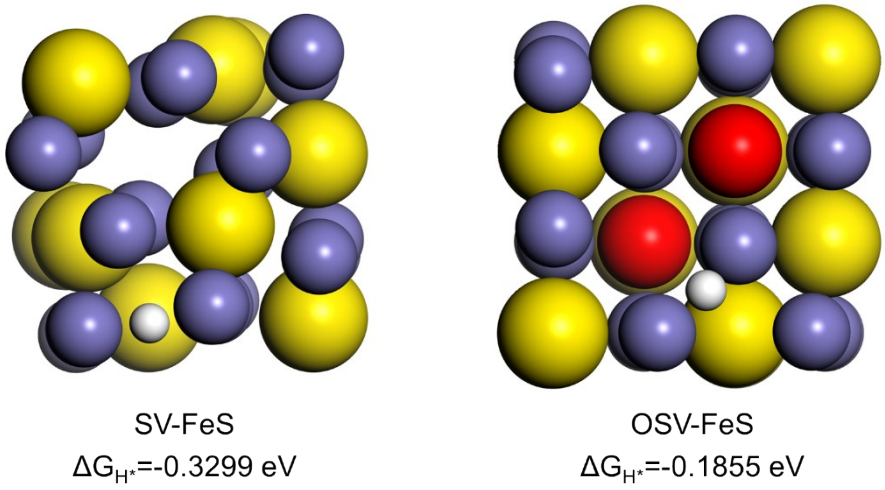

Fig. S19. Representative atomic configurations with corresponding ΔG_{H^*} after H* adsorption at the Fe sites of SV-FeS and OSV-FeS models, respectively.

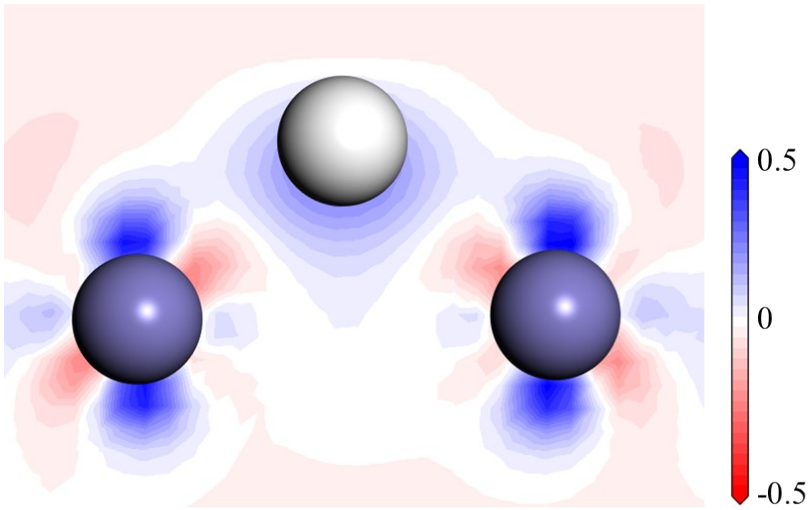

Fig. S20. DFT results of 2D electron density differences after adsorption of H* onto Fe-Fe bridge sites of SV-FeS model. Red and blue represent the depletion and accumulation of electrons with the unit of e Å^{-3}, respectively.

Table S1. ICP results of Fe and S in OSV-FeS electrocatalyst.

Elements	*Mass fraction*	*Atomic content*
Fe	33.4910%	50.9%
S	18.4739%	49.1%

Table S2. ECSA of p-FeS, SV-FeS and OSV-FeS electrode, the mass of catalysts is 0.3 mg cm^{-2}.

Electrode	C_{dl} *(mF* cm^{-2}*)*	*ECSA* (m^2 g^{-1})
p-FeS	6.98	0.582
SV-FeS	16.3	1.358
OSV-FeS	33.6	2.80

Table S3. BET surface area of p-FeS, SV-FeS and OSV-FeS electrocatalysts.

Electrocatalysts	*BET surface area* (m^2 g^{-1})	*Total pore volume* (cm^3 g^{-1})
p-FeS	14.80	0.0496
SV-FeS	57.40	0.129
OSV-FeS	58.25	0.132

Table S4. Performance comparison of recently reported FeS-based HER catalysts.

Catalysts	η_{10} *(mV)*	J_{-200} *(-mA cm^{-2})*	*Tafel slope*	*catalyst Loading (mg cm^{-2})*	*Year*	*Ref.*
Metal-phase FeS	142	30*	37	/	2019	S9
B-Fe_7S_8/FeS_2	113	19*	57	1.8	2022	S10
$FeCo(NiS_2)_4$-C/A	82	90*	70	2.5	2022	S11
Fe_3O_4-FeS/IF	128	72*	90	0.13	2022	S12
FeMoSN@NC	40	29*	67	0.4	2022	S13
H-Fe-CoMoS	138	35*	98	0.4	2020	S14
P-$(Ni,Fe)_3S_2$/NF	98	73*	88	2.90±0.1	2020	S15
$Fe_{0.9}Ni_{2.1}S_2$@NF	72	52*	71	/	2020	S16
FeS_2/CoS_2	78	100*	44	0.28	2018	S17
meso-Fe-MoS_2/$CoMo_2S_4$	122	49*	90	0.6-0.7	2020	S18
FeS_2@1T-MoS_2	161	16*	56	0.3	2023	S19
FeS/Fe_3C@N-S-C-	446	1*	95	/	2018	S20
FeS-H_2 cat	100*	25*	77	/	2018	S21
$Fe_{4.5}Ni_{4.5}S_8$	190	25*	93*	1.5-2.0	2018	S22
OSV-FeS	**72**	**92***	**82**	**0.3**	**-**	**This work**

*Data were estimated according to the curves reported in the paper. η_{10} is the overpotential required at 10 mA·cm^{-2}, j_{-200} is the current densities delivered at -200 mV.

Table S5. Fitted parameters for the equivalent circuit model for p-FeS, SV-FeS and OSV-FeS electrocatalysts.

Parameter	**p-FeS**	**SVs-FeS**	**OSV-FeS**
R_0 (ohm/cm^2)	7.973	4.499	4.998
CPE-T (F/cm^2)	1.0032×10^{-5}	1.0025×10^{-5}	7.4809×10^{-6}
CPE-P	1.0000	0.9998	1.0000
R_{ct} (ohm/cm^2)	104.90	46.98	39.98

References

S1. H. Chen, Z. L. Zhang, Z. L. Yang, Q. Yang, B. Li and Z. Y. Bai, *Chem. Eng. J.*, 2015, **273**, 481-489.

S2. Z. X. Zhu, L. Luo, Y. X. He, M. Mushtaq, J. Q. Li, H. Yang, Z. Khanam, J. Qu, Z. M. Wang and M. S. Balogun, *Adv. Funct. Mater.*, 2024, **34**, 2306061.

S3. T. Z. Xiong, Z. X. Zhu, Y. X. He, M. S. Balogun and Y. C. Huang, *Small Methods*, 2023, **7**, 2201472.

S4. S. J. Clark, M. D. Segall, C. J. Pickard, P. J. Hasnip, M. J. Probert, K. Refson and M. C. Payne, *Z. Kristall*, 2005, **220**, 567-570.

S5. J. P. Perdew, K. Burke and M. Ernzerhof, *Phys. Rev. Lett.*, 1997, **78**, 1396-1396.

S6. D. Vanderbilt, *Phy. Rev. B*, 1990, **41**, 7892-7895.

S7. H. J. Monkhorst and J. D. Pack, *Phy. Rev. B*, 1976, **13**, 5188-5192.

S8. J. K. Norskov, T. Bligaard, A. Logadottir, J. R. Kitchin, J. G. Chen and S. Pandelov, *J. Electrochem. Soc.*, 2005, **152**, J23-J26.

S9. G. Zhou, Y. Shan, L. L. Wang, Y. Y. Hu, J. H. Guo, F. R. Hu, J. C. Shen, Y. Gu, J. T. Cui, L. Z. Liu and X. L. Wu, *Nat. Commun.*, 2019, **10**, 399.

S10. J. Wu, Q. Zhang, K. Shen, R. Zhao, W. D. Zhong, C. F. Yang, H. Xiang, X. K. Li and N. J. Yang, *Adv. Funct. Mater.*, 2022, **32**, 2107802.

S11. Z. X. Gu, Y. C. Zhang, X. L. Wei, Z. Y. Duan, L. Ren, J. C. Ji, X. Q. Zhang, Y. X. Zhang, Q. Y. Gong, H. Wu and K. Luo, *Adv. Sci.*, 2022, **9**, 2201903.

S12. M. Yang, W. H. Hu, M. X. Li, Y. N. Cao, B. Dong, Y. Ma, H. Y. Zhao, F. G. Wang, J. Huang and Y. M. Chai, *J. Energy Chem.*, 2022, **68**, 96-103.

S13. X. H. Xia, G. Y. Zhao, Q. Yan, B. Wang, Q. F. Wang and H. J. Xie, *ACS Sustainable Chem. Eng.*, 2022, **10**, 182-193.

S14. Y. N. Guo, X. Zhou, J. Tang, S. Tanaka, Y. V. Kaneti, J. Na, B. Jiang, Y. Yamauchi, Y. S. Bando and Y. Sugahara, *Nano Energy*, 2020, **75**, 104913.

S15. C. C. Liu, D. B. Jia, Q. Y. Hao, X. R. Zheng, Y. Li, C. C. Tang, H. Liu, J. Zhang and X. L. Zheng, *ACS Appl. Mater. Interfaces*, 2019, **11**, 27667-27676.

S16. B. Fei, Z. L. Chen, J. X. Liu, H. B. Xu, X. X. Yan, H. L. Qing, M. Chen and R.

B. Wu, *Adv. Energy Mater.*, 2020, **10**, 2001963.

S17. Y. N. Guo, J. Tang, J. Henzie, B. Jiang, W. Xia, T. Chen, Y. Bando, Y. M. Kang, S. A. Hossain, Y. Sugahara and Y. Yamauchi, *ACS Nano*, 2020, **14**, 4141-4152.

S18. K. Wang, K. Yu, S. Xu, S. Yuan, L. Xiang, B. Pang, J. Zheng and N. Li, *Appl. Catal. B: Environ.*, 2023, **328**, 122445.

S19. F. T. Kong, X. H. Fan, A. G. Kong, Z. Q. Zhou, X. Y. Zhang and Y. K. Shan, *Adv. Funct. Mater.*, 2018, **28**, 1803973.

S20. X. X. Zou, Y. Y. Wu, Y. P. Liu, D. P. Liu, W. Li, L. Gu, H. Liu, P. W. Wang, L. Sun and Y. Zhang, *Chem*, 2018, **4**, 1139-1152.

S21. C. L. Bentley, C. Andronescu, M. Smialkowski, M. Kang, T. Tarnev, B. Marler, P. R. Unwin, U. P. Apfel and W. Schuhmann, *Angew. Chem. Int. Ed.*, 2018, **57**, 4093-4097.

S22. Y. V. Lim, S. Z. Huang, Y. M. Zhang, D. Z. Kong, Y. Wang, L. Guo, J. Zhang, Y. M. Shi, T. P. Chen, L. K. Ang and H. Y. Yang, *Energy Storage Mater.*, 2018, **15**, 98-107.